Journal of Materials Chemistry C

Accepted Manuscript

ROYAL SOCIETY OF CHEMISTRY

rsc.li/materials-c

View Article Online
DOI: 10.1039/C9TC00311H

Materials Chemistry C

ARTICLE

Sol-gel magnetite inks for inkjet printing

Denis S. Kolchanov[a], Vladislav Slabov [a], Kirill Keller [a] Ekaterina Sergeeva [a], Mikhail V. Zhukov [a,b], Andrey S. Drozdov [a]*, Alexandr V. Vinogradov [a]

Received 00th January 20xx,
Accepted 00th January 20xx

DOI: 10.1039/x0xx00000x

www.rsc.org/

The article describes easy-to-implement and print-ready composition for inkjet printing of magnetic structures, which can be used for security printing, coding, and marking, magnetic devices fabrication or creation of micro-antennas. The synthesized inks are based on biocompatible stable magnetite hydrosol and consists of monodisperse magnetite nanoparticles. The ink composition was optimized in order to ensure stable printing; the optimal printing conditions were achieved using the theory of Ohnesorge and by optimization of a piezoelectric waveform. In addition, the influence of substrate material on drop formation was studied. The magnetic properties of the printed samples were measured using magnetic force microscopy (MFM). Printed thin magnetite films showed good magnetic properties, and therefore the ink can be used for printing of anti-counterfeiting magnetic patterns.

Introduction

Nowadays, an increasing number of methods and technologies is used to protect brands and valuable documents from falsifications[1–3]. Most of the anti-counterfeiting approaches include unique marking (e.g., watermarks, holograms, individual numbers, etc.), but their production is expensive. Inkjet printing for a long time was of great interest for rapid and cost-efficient coding and marking[4]. However, in recent years, it is also increasingly used in the field of protective holographic coatings that require individual design, as it is an excellent alternative to the variety of lithographic methods, micro-embossing, and PVD processes, which require fabrication of new physical template to change the vector of production[5,6].

Inkjet printing is an additive technology that allows selective deposition of coatings without the need to create pre-patterns such as templates and masks, which is the case in lithography or screen printing[7]. The inkjet printing technology is actively used in research because it has available components for its implementation (the printhead, ink and the medium for imaging), which give a possibility to study and development different functional materials and coverings. The ability to use stretchable and flexible polymeric substrates is a distinctive feature of inkjet printing, beneficial for the development of cost-effective, flexible electronics[8–10]. Several examples of optical anti-counterfeiting systems are known from the literature[11–13], but despite the constant development of security technologies, the market is increasingly requiring extra protection, and optical structures may be of interest to improve the security of documents. For example, additional protection of the documents can be obtained by a deposited magnetic code or including unique protective patterns with a various number of layers resulting in a different magnetic response.

Recent advances of magnetic recording technologies[14,15], associated with an increase in density of the magnetic recording and, as a consequence, an increase in memory bits, the development of micro-dimensional sensor devices[16] of the resonant type for the detection of micromagnetic fields, make inkjet printing of magnetic structures extremely promising application[17].

It was shown that printed magnetic films are perspectives materials for cores of RFID resonators[18] or the formation of microscale structures[19]. However, nowadays implementation of inkjet printing technique for magnetic applications is limited by a number of factors, including the difficulties in the synthesis of stable colloids of magnetic nanoparticles and adaptation of their rheological parameters. In most cases, magnetic nanoparticles are synthesized via hydrothermal synthesis or high-temperature decomposition of organic precursors including iron pentacarbonyl, or high-temperature synthesis in polyols[20,21]. In most cases a further modification of the nanoparticles surface is required in order to enhance the colloidal stability of the system, leading to increased costs of the production and limiting the potential areas of application of such inks.

To overcome these hurdles, we describe the cost-efficient magnetite-based inks for inkjet printing prepared from a stable magnetite hydrosol[22,23] with a subsequent optimization of its rheological and surface tension parameters. Proposed magnetic inks are cheap, easy to produce, have a non-aggressive and non-toxic composition and show high magnetization values and stability. Influence of substrate materials on the morphology of printed structures was comprehensively studied, especially, the

[a] ITMO University, 191002, Lomonosova st. 9, Saint Petersburg, Russian Federation
[b] Institute for Analytical Instrumentation RAS, 198095 Ivan Chernykh st., 31-33, Saint Petersburg, Russian Federation

* drozdov@scamt-itmo.ru

† Footnotes relating to—— the title and/or authors should appear here.
Electronic Supplementary Information (ESI) available: [details of any supplementary information available should be included here]. See DOI: 10.1039/x0xx00000x

View Article Online
DOI: 10.1039/C9TC00714H

influence of the contact angle on the particle distribution over the substrate surface in a printed drop. Highly pronounced magnetic properties investigated using MFM method allow using magnetite-based inks in a wide range of applications.

Experimental section

Materials

Iron (II) chloride tetrahydrate (99%), iron (III) chloride hexahydrate (97%), ammonia 25% solution in water, diethylene glycol were all purchased from Sigma Aldrich and used without any further purification. As substrates for printing silicon wafer (size 0.5 mm, roughness 1 nm) and PET film (Milinex PCS 125 micron) were obtained from Sigma Aldrich, glass slides (size 76 mm × 25 mm × 1 mm, roughness < 50 nm) were obtained from Levenhuk.

Synthesis of nanoparticles of magnetite

2.5 g $FeCl_2$ $4H_2O$ and 5 g $FeCl_3$.$6H_2O$ (Fe^{2+}/Fe^{3+} molar ratio of 0.7) were dissolved in 100 mL of deionized water under constant stirring (500 rpm). Then 12 mL of an aqueous ammonia solution was added to this solution at room temperature and constant stirring. A precipitate was collected using a magnet and washed with deionized water until neutral pH. The washed black precipitate was mixed with 100 mL of deionized water and ultrasonicated (37 kHz, 110 W) with constant stirring at 300 rpm for 120 min. The obtained magnetite sol was then cooled to room temperature. The mass fraction of the magnetite sol was 2.2%.

Ink preparation and printing

The ink was obtained by mixing variable volumes of magnetite sol with diethylene glycol. The solution was thoroughly mixed and cleaned of possible impurities using a filter with a pore size of 0.45 µm before loading into the cartridge. The cartridge was degassed in the desiccator under vacuum to avoid the formation of residual air bubbles during the printing.

Printing of magnetite-based inks was performed on R&D Fujifilm Dimatix Materials Printer DMP (2831) using Dimatix Materials cartridges with a drop volume of 10 pL. The DMP-2831 model has A4 size substrate table with a vacuum pump and heating possibility up to 60°C.

The waveform designed for inkjet printing of magnetite ink is presented in Figure S1. Printing was performed at room temperature 25 degrees without drying between layers; the drop spacing was 60 µm

Characterization

The hydrodynamic radius and zeta potential were measured with a particle size analyzer Photocor Compact-Z. The X-ray diffraction (XRD) analysis was performed with Bruker D8 Advance using Cu-Kα radiation (λ = 1.54 Å). The samples were scanned for 2 h at a rate of 0.5 degrees/min. For a scanning electron microscopy (SEM) analysis the samples were dried under vacuum for 1 h and examined without additional metal coating using a Magellan 400L and Tescan VEGA 3 scanning electron microscopes. The transmission electron microscopy (TEM) was obtained on FEI TECNAI G2 F20, at an operating voltage of 200 kV. The Raman spectra were recorded using the 633 nm He-Ne laser line on a Horiba Jobin-Yvon MicroRaman 300 spectrometer. The laser power on the samples employed was 0.030 mW and 0.344 mW, with 300 s and 120 s exposition per diffraction window, respectively. In all the measurements, 50x Olympus lens, hole of 500 mm, slit of 100 mm and a diffraction grid with a period 1800 grooves/mm were employed. Topographic atomic force microscopy and MFM were made on NT MDT Solver Next microscope. MFM01 probes (NT-MDT, Russia) with 30-40 nm thick magnetic coating of CoCr and a typical radius of tip curvature about 40 nm were used [AD1]. The typical MFM probe resonance frequency was about f0 ≈ 70 kHz.

Rheological measurements were performed on rotational viscometer Fungilab Expert with a small sample adapters APM. The surface tension of produced inks and contact angle for different substrates were measured on drop shape analyzer KRUSS DSA 25.

Results and Discussion

Magnetite nanoparticles

As the basis for magnetic inks, we have chosen biocompatible stable Magnetite hydrosol capable of undergoing a sol-gel transition at room temperatures[22,23]. The hydrosol was synthesized by co-precipitation procedure using a mixture of iron (II) and iron (III) chlorides and water-ammonia solution as a base. After co-precipitation, the mixture was magnetically separated and washed to neutral pH level with subsequent ultrasonic (US) treatment (see Experimental section for the details). Upon US irradiation, disaggregation of the black precipitate was observed with the formation of a black non-transparent hydrosol. The obtained hydrosol was stable under the ambient conditions and had a shelf-life for at least one month without notable precipitation. The hydrosol behaved like a typical magnetic fluid: in the presence of an external magnetic field it was attracted to a magnet without notable phase separation (Figure 1a), the mass fraction of solids in the hydrosol was estimated on the level of 2% wt. The hydrosol consisted of nanoparticles composed of magnetite crystalline phase which was proved with XRD analysis (Figure 1b) and Raman spectroscopy (Figure 1c). The nanoparticles had a mean particle diameter of 10±2 nm which was estimated with XRD analysis (Figure 1b) and were visualized with TEM (Figure 1d) and SEM (Figure 1e). The excellent colloidal stability of the magnetite nanoparticles in aqueous media at neutral pH was ensured by a highly positive zeta potential of the system up to +36 mV, resulting in electrostatic repulsive force and preventing the nanoparticles from coagulation. The high value of the zeta potential originated from the surface chemistry of the nanoparticles: the presence of Fe(II)-OH hydroxyl groups on their surface shifted the isoelectric point of the system to pH 8.3 (Figure S3)[24,25].

The absence of any stabilizing coatings and peptizing agents in combination with excellent colloidal stability allowed the nanoparticles to undergo the sol-gel transition upon solvent removal under mild conditions leading to the formation of the

View Article Online
DOI: 10.1039/C9TC00311H

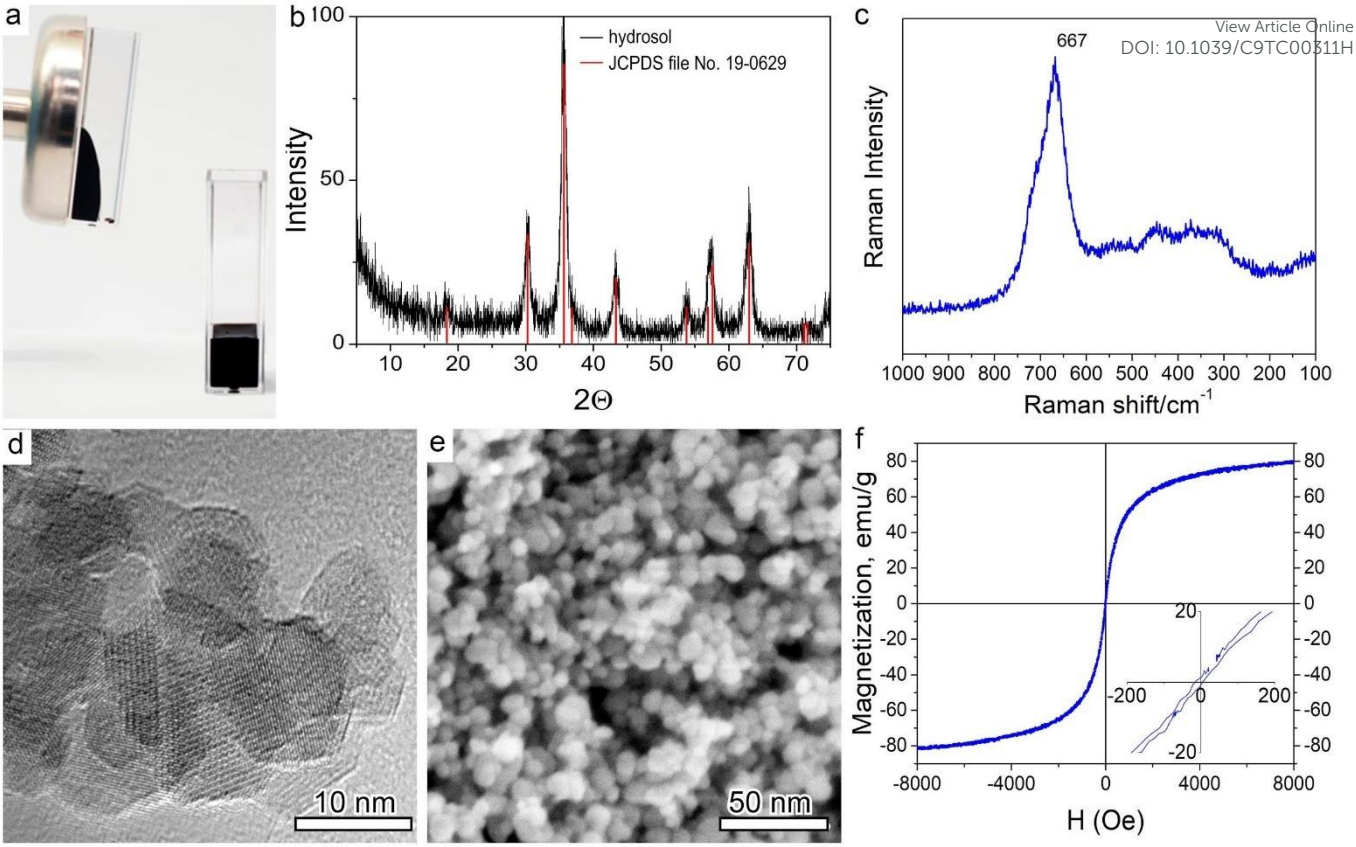

Figure 1 – Magnetite hydrosol a) visual appearance of the magnetite hydrosol; b) XRD pattern of the magnetite hydrosol; c) Raman spectra of the hydrosol, single peak at 667 cm^{-1} is typical for magnetite oxide form; d) TEM image of the magnetite hydrosol; e) SEM image of the hydrosol; f) magnetization curve of the sample, absence of the magnetization curve hysteresis can be seen in insert

rigid inorganic matrix. The matrix showed a mesoporous structure with the mean pore diameter of 8 nm and a total surface area of 120 m^2/g and was stable after subsequent treatment with water without any signs of resuspension. The material showed superparamagnetic behavior with magnetization up to 79 emu/g at 8000 Oe, which is close to the bulk magnetite (Figure 1f).

Two-component composition, scalable and straightforward synthetic procedure and high mass fractions of magnetite nanoparticles made the synthesized hydrosol a prospective candidate to be used as a main component for magnetic inks. However, the rheological parameters of the system need to be optimized to meet the requirements for inkjet printing.

Rheology and composition of the magnetic inks

In present work, the influence of the solvent concentration in magnetite sol on the rheological parameters of the ink was studied. To be printable, the inks ought to demonstrate high colloidal stability and proper rheological and dynamical fluid characteristics, which could be described by Reynolds (Re) and Ohnesorge (Oh) numbers:

$$Re = \frac{\rho V d}{\eta} \quad (1)$$

$$Oh = \frac{\eta}{\sqrt{\gamma \rho d}} \quad (2)$$

where ρ, η, γ are density, viscosity and surface tension of prepared inks respectively, V is the velocity of the jetted drop and d is a diameter of printhead nozzle[26]. In Dimatix cartridges d =21 µm. Reynolds number represents the ratio between inertial and viscous forces, while the Ohnesorge number describes a relationship between viscosity and surface tension without considering driving forces. Considering that, for stable drop generation, the parameter Z=1/Oh should be in the range $10 > Z > 4$[27]. Since magnetite sol is water-based, its rheological properties are not suitable for the inkjet printing technology. Thus, additional solvents for viscosity adjustment and surfactants for reduction of surface energy should be used. Diethylene glycol was chosen for this purposes due to its high viscosity (35.7 cPs) and low surface tension (44 mN/m). Various inks compositions were evaluated in order to find the optimal ratio between the magnetite sol and diethylene glycol. Table 1 shows the essential ink parameters influencing the printing process. It can be observed that all rations are suitable for inkjet printing. However, the ratio 2:1 magnetite sol/diethylene glycol was chosen for printing because this ink has the maximal concentration of magnetite sol and therefore its maximal concentration in printed drops. Besides that, an increase in the concentration of diethylene glycol leads to a change in the dielectric constant of the liquid medium, and as affects the ζ-potential of the system, resulting in alternations of its stability (Table 1). The ink has excellent coagulation stability for more

Table 1 - The main parameters of prepared inks

View Article Online
DOI: 10.1039/C9TC00311H

Magnetite sol/Diethylene glycol ratio	Viscosity, cPs	Surface tension, mN/m	Re	We	Oh	Z	ζ – potential, mV
1:0	1.2	61.09 + 2,18	140.0	22.1	0.03	29.8	31.6 ± 0.3
2:1	3.1	44.83 + 0.4	54.2	30.5	0.10	9.8	25.2 ± 0.1
1:1	4.6	40.25 + 0.14	36.5	33.6	0.16	6.3	21.3 ± 0.5
1:2	6.4	37.79 + 0.59	26.2	35.3	0.23	4.4	18.4 ± 0.2
1:3	8.0	36.83 + 0.12	21.0	36.3	0.29	3.4	16.9 ± 0.1

than 30 days as it was demonstrated by the DLS measurements. The change of the hydrodynamic radius of the nanoparticles did not exceed 10% after a month on the shelf (Figure S5).

Inkjet printing of magnetic samples

The inks with optimized magnetite content were printed on various substrates (silicon wafer, PET film and glass slides) study the influence of the surface properties on the drop formation and distribution of magnetite particles. Contact angles of the ink on different substrates (Figure 2a) are in good correlations with the diameter of the dried printed drops as it can be seen from SEM images (Figure 2b). Depending on the substrate surface energy, deposited ink drops have different diameters resulting in variations of magnetite particles distribution on the substrate surface.

The smooth surface of monocrystalline silicon substrates (surface mean roughness Ra = 1.01±0.54 nm according to performed AFM measurements) is covered with a thin oxide film SiO2 and functional silanol groups (Si-OH), which have a high level of interaction with polar water molecules. Therefore, nearly uniform and defect-less coatings of magnetic particles were formed on a surface of monocrystalline silicon. The glass substrate surface has the same functional groups as the silicon substrate. Nevertheless, the higher roughness of glass substrates (Ra = 5.09 ± 0.28 nm according to AFM measurements) and glass production-associated inorganic impurities leads to the formation of a significant number of irregularities and defects during the self-assembling of magnetite nanoparticles. Since drops on the PET film (Ra = 0.58 ± 0.12 nm according to AFM measurement) have the highest contact angle and due to the low polarity of its surface, ink particles distribute more evenly on the surface that can be useful for the formation of small concentrated areas of deposited material[28].

Magnetic properties of printed structures were investigated using a magnetic force microscopy technique. This method relies on two-pass technique in the phase contrast mode with the measurement of phase shift arising between oscillations of a piezo vibrator and oscillations of a probe in the presence of a

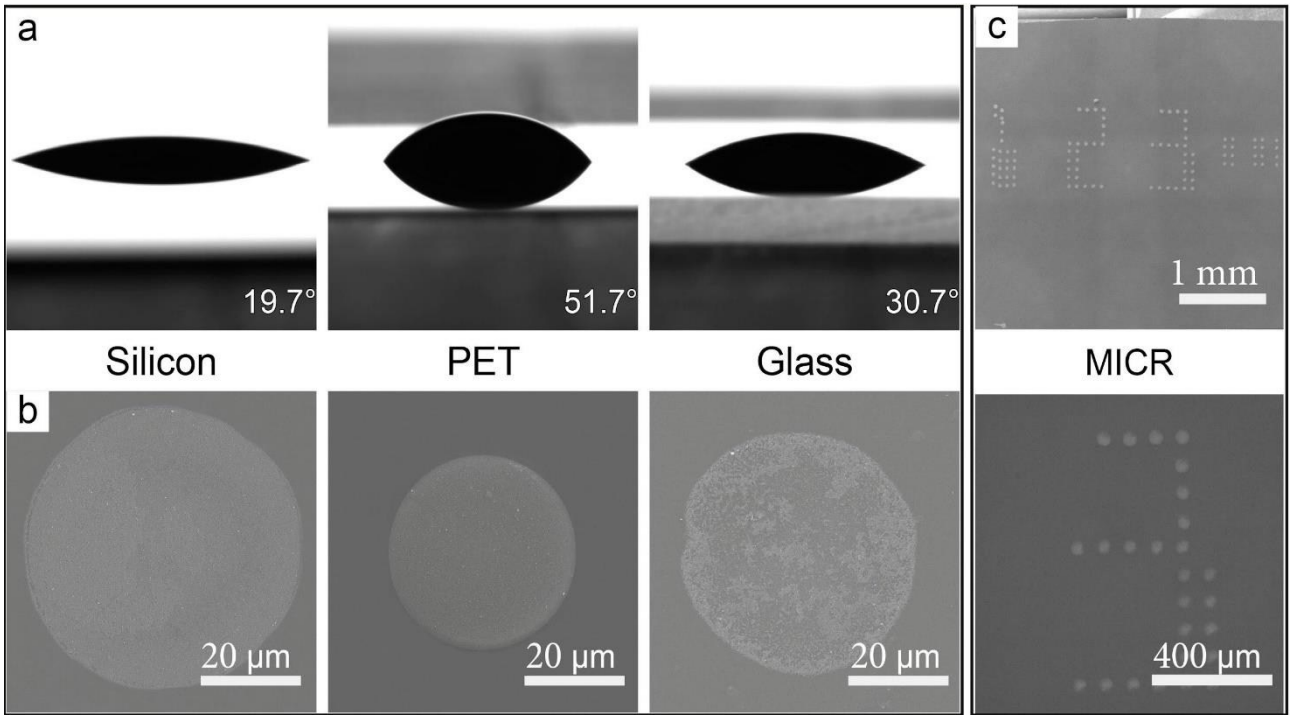

Figure 2 – SEM images of a) ink drop on different surfaces and their contact angles and b) SEM of drops deposited onto different surfaces c) printed MICR characters

View Article Online
DOI: 10.1039/C9TC00311H

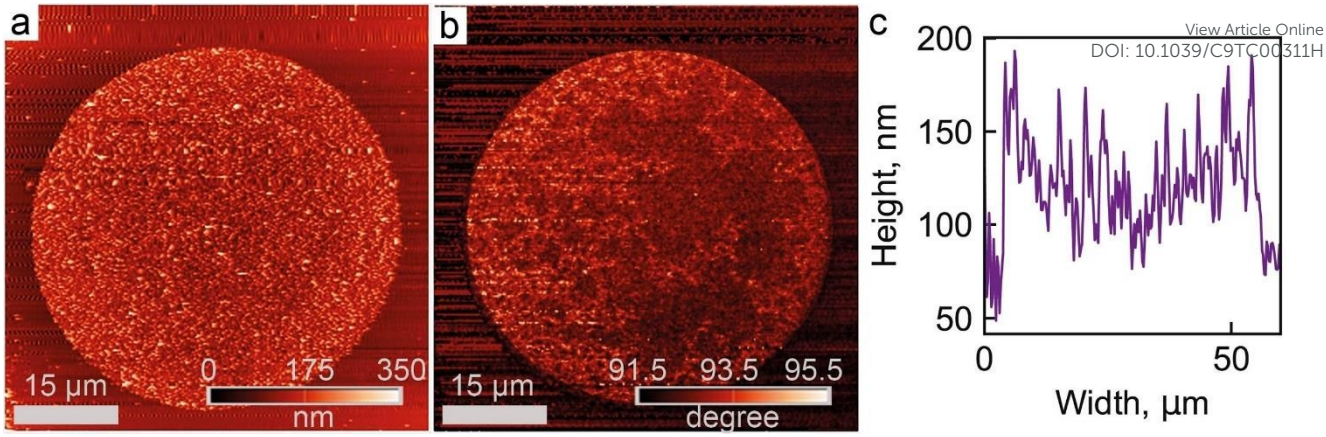

Figure 3 – Images of a) AFM of the drop surface b) MFM of the deposited magnetite drop c) cross-section profile of the drop on the silicon substrate

magnetic field gradient (Table 2)[29]. The first pass extracts information about the topography (Figure 3a), while during the second pass magnetic forces have been registered at a fixed distance from the surface of the sample (characterized by $\Delta Z \approx 10$ nm) (Figure 3b).

The magnetic force is determined by measuring the gradient of the probe magnetic moment interaction energy with the magnetic field of the sample. It depends on the gradient of the magnetic field of the sample and the interdependence of the magnetic moment of the probe from coordinates[30].

The presence of the force gradient $F'z$ leads to a shift of the resonant frequency and phase[29] of the probe oscillations, determined by the properties of the probe and the magnetic field of the sample (Table 2).

It is known[29] that the phase shift between oscillations of a piezo vibrator and oscillations of a probe in an MFM is determined by the quality factor of the cantilever Q, its stiffness k and the gradient of the magnetic force F'_z between the probe and the specimen in the Z direction perpendicular to the sample plane:

$$\delta(a) = \frac{Q \times F'_z}{k} \quad (3)$$

Magnetic properties were studied for samples printed on the silicon having 1 to 3 layers (Figure S2). The magnetic response depends on the amount of magnetite in the dried drop. Particle distribution in the center of the printed drop is homogenous which contributes to a higher magnetic field than on the drop edges (coffee ring) which characterized by the changes of the phase shift of the probe (Figure S4)).

Table 2 – Phase probe oscillations on deposition drops

	Phase probe oscillations, degrees		
	on the drop edges	drop center	average value
1 layer	1.5	1.7	1.6
2 layers	1.7	2.0	1.9
3 layers	2.0	2.2	2.1

The gradient of the magnetic force was calculated using measured phase shift applying equation (3), typical Q-factor of the probe about 200 and the value of the probe stiffness measured by the Sader method[31] is k = 2 N/m (Table 3).

The obtained results confirm that using drop-on-demand printing allows the formation of a thin uniform magnetite layer. While the thickness of the deposited layers (controlled by the number of passes) linearly influence its magnetic response

Inkjet holographic pattering

One of the specific applications of magnetite printing is holographic protection, which can be used for additional coding and document protection. The working principle of this technology was described in detail by Yakovlev et al.[32]. Here, the

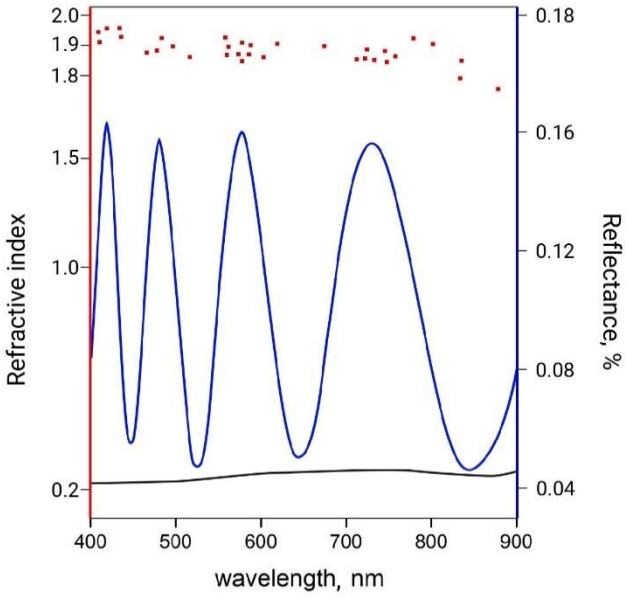

Figure 4 – Dispersion of the refractive index for Fe3O4 inkjet film (red square) and reflection spectrum of a 500 nm thick Fe3O4 inkjet film on a 2 mm fused silica substrate in the air (black solid line); reflection from fused silica substrate (black line).

View Article Online
DOI: 10.1039/C9TC00311H

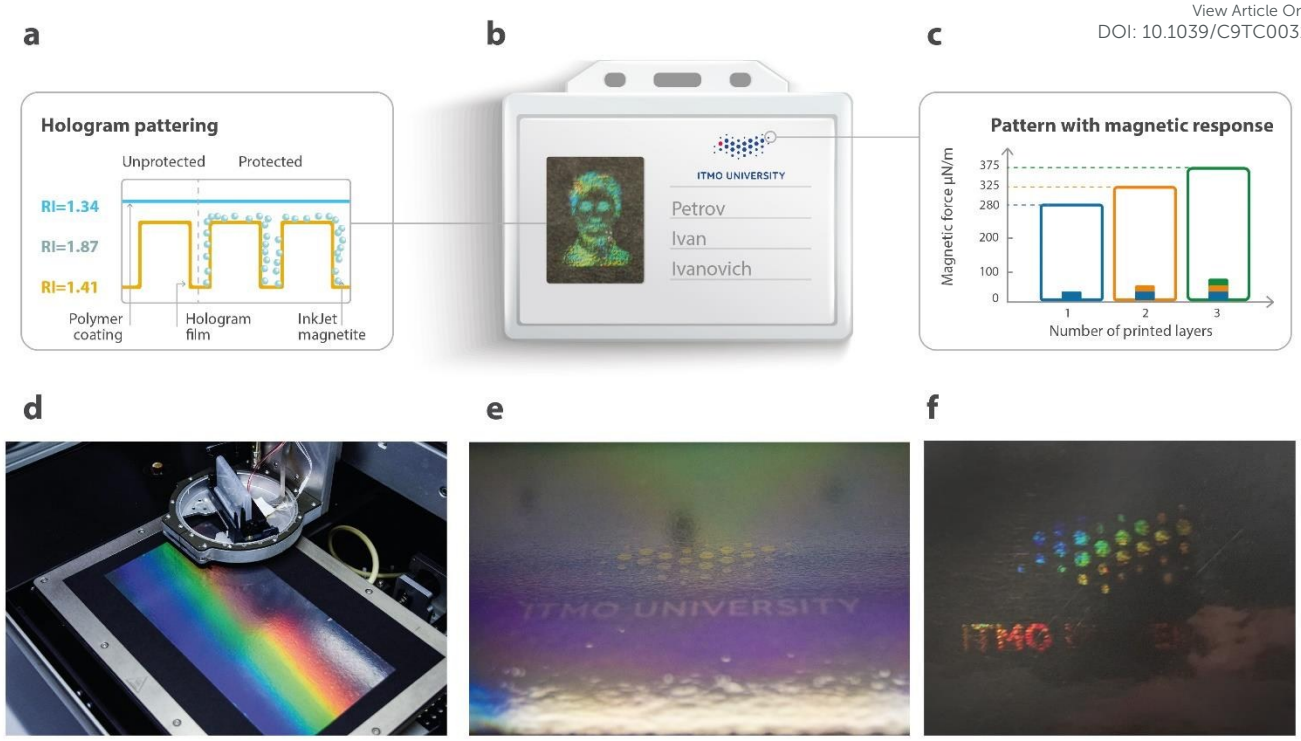

Figure 5 – Concept art of security printing a) holographic protection c) magnetic pattern with the various number of layers and magnetic response. Inkjet holographic pattering d) holographic foil e) printed of high refractive magnetite nanoparticles f) laminated with a polymer layer.

material with high refractive index (n > 1.7) is deposited on the microrelief of hot-embossed holographic paper having a lower refractive index of n = 1.41. The optical properties of magnetite, such as refractive index dispersion and reflectance spectrum, are shown in Figure 4. Magnetite ink has a refractive index of n=1.87 ± 0.05 in a visible light spectrum. Therefore, a thin magnetite layer can serve as a masking layer by further lamination with a polymer with refractive index n=1.34 (Figure 5a) which is close to the value of refractive index of the holographic paper.

Table 3 – The gradient of magnetic forces the dependence of magnetic force at the number of layers

System	Magnetic forces, μN/m		
	on the drop edges	drop center	average value
1 layer	260	**300**	280
2 layers	300	**350**	325
3 layers	330	**420**	375

A thin magnetite layer is selectively deposited on the surface of holographic paper by means of inkjet printing. Figure 5 d-f demonstrates the process flow of inkjet printing of protective magnetite layer. The used printing parameters are given in the Supplementary section. In the following step, the holographic paper with deposited magnetite layer is laminated with low refractive index polymer. As a result, the holographic response of the foil is preserved only in the regions protected with thin magnetite layer.

Conclusion

In this work, we described a simple low-temperature synthesis of the magnetic inks based on biocompatible magnetite nanoparticles. Inks composition and rheological properties were optimized based on the Ohnesorge theory. Optimal conditions were found between maximal magnetite nanoparticles concentration and stable jetting performance for large-scale printing of magnetic microstructures. Inkjet printing was carried out on glass, PET film, and silicon substrates to study the influence of surface properties on the distribution of magnetite particles in dried layers. In this work, it has been shown the investigation of inkjet printed systems with magnetic force microscopy that showed the best average magnetic response in samples printed in three passes, due to the best distribution of particles on the surface of the material. We have investigated the optical properties of printed thin magnetite film. Our findings in inkjet printing of magnetite inks on flexible substrates have direct application for information coding and anti-counterfeiting purposes, which was confirmed in our paper. We believe that our work will significantly affect existing fabrication technologies of magnetic devices.

Conflicts of interest

There are no conflicts to declare.

Acknowledgments

This work was supported by the Russian Science Foundation Grant No. 16-19-10346.

Bibliography

1 D. Bansal, S. Malla, K. Gudala and P. Tiwari, *Scientia Pharmaceutica*, 2012, **81**, 1–14.
2 A. Hoecht and P. Trott, *Int Journal of Emerging Mkts*, 2014, **9**, 98–119.
3 B. Yoon, J. Lee, I. Sung Park, S. Jeon, J. Lee and J.-M. Kim, *Journal of Materials Chemistry C*, 2013, **1**, 2388–2403.
4 S. Magdassi, Ed., *The Chemistry of Inkjet Inks*, World Scientific Pub Co Inc, Singapore ; Hackensack, NJ, 2009.
5 J. Andres, R. D. Hersch, J.-E. Moser and A.-S. Chauvin, *Advanced Functional Materials*, 2014, **24**, 5029–5036.
6 M. You, J. Zhong, Y. Hong, Z. Duan, M. Lin and F. Xu, *Nanoscale*, 2015, **7**, 4423–4431.
7 S. D. Hoath, *Fundamentals of Inkjet Printing*, Wiley-VCH Verlag GmbH & Co., Weinheim, Germany.
8 Q. Huang and Y. Zhu, *Advanced Materials Technologies*, 2019, 1800546.
9 D. McManus, S. Vranic, F. Withers, V. Sanchez-Romaguera, M. Macucci, H. Yang, R. Sorrentino, K. Parvez, S.-K. Son, G. Iannaccone, K. Kostarelos, G. Fiori and C. Casiraghi, *Nature Nanotechnology*, 2017, **12**, 343–350.
10 S. G. Hashmi, D. Martineau, X. Li, M. Ozkan, A. Tiihonen, M. I. Dar, T. Sarikka, S. M. Zakeeruddin, J. Paltakari, P. D. Lund and M. Grätzel, *Advanced Materials Technologies*, 2016, 2(1) 160183,
11 K. Keller, A. V. Yakovlev, E. V. Grachova and A. V. Vinogradov, *Advanced Functional Materials*, 2018, **28**, 1706903.
12 V. Slabov, A. V. Vinogradov and A. V. Yakovlev, *Journal of Materials Chemistry C*, 2018, **6**, 5269–5277.
13 A. V. Yakovlev, V. A. Milichko, V. V. Vinogradov and A. V. Vinogradov, *ACS nano*, 2016, **10**, 3078–3086.
14 S. Dey, K. Mohanta and A. J. Pal, *Chemical Physics Letters*, 2010, **492**, 281–284.
15 G. Ju, Y. Peng, E. K. C. Chang, Y. Ding, A. Q. Wu, X. Zhu, Y. Kubota, T. J. Klemmer, H. Amini, L. Gao, Z. Fan, T. Rausch, P. Subedi, M. Ma, S. Kalarickal, C. J. Rea, D. V. Dimitrov, P.-W. Huang, K. Wang, X. Chen, C. Peng, W. Chen, J. W. Dykes, M. A. Seigler, E. C. Gage, R. Chantrell and J.-U. Thiele, *IEEE Transactions on Magnetics*, 2015, **51**, 1–9.
16 D. F. Wang and R. Maeda, *Microsystem Technologies*, 2015, **21**, 1167–1172.
17 X. Zhou, C. Fang, Y. Li, N. An and W. Lei, *Composites Part B: Engineering*, 2016, **89**, 295–302.
18 N. Marjanović, A. Chiolerio, M. Kus, F. Ozel, S. Tilki, N. Ivanović, Z. Rakočević, V. Andrić, T. Barudžija and R. R. Baumann, *Thin Solid Films*, 2014, **570**, 38–44.
19 W. Voit, W. Voit, L. Belova, W. Zapka and K. V. Rao, *IEE Proceedings - Science, Measurement and Technology*, 2003, **150**, 252–256.
20 W. Cai and J. Wan, *Journal of Colloid and Interface Science*, 2007, **305**, 366–370.
21 P. Nadoll, T. Angerer, J. L. Mauk, D. French and J. Walshe, *Ore Geology Reviews*, 2014, **61**, 1–32.
22 Y. I. Andreeva, A. S. Drozdov, A. F. Fakhardo, N. A. Cheplagin, A. A. Shtil and V. V. Vinogradov, *Scientific Reports*, 2017, **7**, 11343.
23 O. E. Shapovalova, A. S. Drozdov, E. A. Bryushkova, M. I. Morozov and V. V. Vinogradov, *Arabian Journal of Chemistry*, DOI:10.1016/j.arabjc.2018.02.011.
24 A. S. Drozdov, V. Ivanovski, D. Avnir and V. V. Vinogradov, *Journal of Colloid and Interface Science*, 2016, **468**, 307–312.
25 E. I. Anastasova, V. Ivanovski, A. F. Fakhardo, A. I. Lepeshkin, S. Omar, A. S. Drozdov and V. V. Vinogradov, *Soft Matter*, 2017, **13**, 8651–8660.
26 B. Derby, *Annual Review of Materials Research*, 2010, **40**, 395–414.
27 D. Jang, D. Kim and J. Moon, *Langmuir*, 2009, **25**, 2629–2635.
28 P.-G. de Gennes, F. Brochard-Wyart and D. Quere, *Capillarity and Wetting Phenomena: Drops, Bubbles, Pearls, Waves*, Springer-Verlag, New York, 2004.
29 Y. Martin, D. Rugar and H. K. Wickramasinghe, *Applied Physics Letters*, 1988, **52**, 244–246.
30 Landau / Lifshitz | The Classical Theory of Fields | 4th edition | 1987, https://www.beck-shop.de/landau-lifshitz-classical-theory-of-fields/productview.aspx?product=473332, (accessed November 24, 2018).
31 M. J. Higgins, R. Proksch, J. E. Sader, M. Polcik, S. Mc Endoo, J. P. Cleveland and S. P. Jarvis, *Review of Scientific Instruments*, 2006, **77**, 013701.
32 A. V. Yakovlev, V. A. Milichko, V. V. Vinogradov and A. V. Vinogradov, *Advanced Functional Materials*, 2015, **25**, 7375–7380.

View Article Online
DOI: 10.1039/C9TC00311H

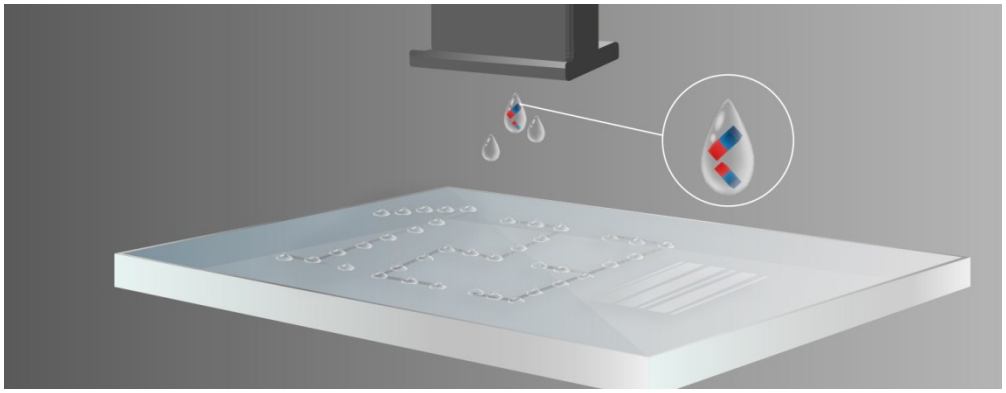

129x50mm (300 x 300 DPI)